Sound & Vibration 2026, 60(5), 4531.
doi: https://doi.org/10.59400/sv4531

Article

Integrated finite element and reduced-order modeling analysis of a real flat top tower crane system

Mustafa Tınkır [1,*], **Ali Çoban** [2]

[1] Department of Mechanical Engineering, Faculty of Engineering, Necmettin Erbakan University, Konya 42090, Turkey
[2] Department of Mechanical Engineering, Faculty of Engineering and Natural Sciences, Konya Technical University, Konya 42250, Turkey; acoban@ktun.edu.tr
* **Corresponding author:** Mustafa Tınkır, mtinkir@erbakan.edu.tr

CITATION

Tınkır M, Çoban A. Integrated finite element and reduced-order modeling analysis of a real flat top tower crane system. Sound & Vibration. 2026; 60(5): 4531
https://doi.org/10.59400/sv4531

ARTICLE INFO

Received: 18 June 2026
Revised: 18 July 2026
Accepted: 27 July 2026
Available online: 16 August 2026

Abstract: This study presents the structural and dynamic analysis of a real 60/15 flat-top tower crane with a free-standing height of 48 m. Finite element analyses were performed to evaluate the stress distribution, deformation, and dynamic characteristics of the main structural components. Based on the finite element results, a 17-degree-of-freedom (17-DOF) reduced-order mathematical model was developed. The stiffness coefficients were obtained from the finite element deformations using Hooke's law, while the damping coefficients were determined analytically. An elastic multibody model of the crane was also developed in MATLAB/SimMechanics to validate the proposed reduced-order model. The finite element analyses showed that the maximum equivalent stress remained below the allowable stress limit (approximately 225 MPa), while the maximum displacement of the mast reached 183.94 mm under the design loading condition. Modal analysis indicated that the counter-jib had the lowest first natural frequency (0.64 Hz), making it the most flexible structural component of the crane. Under the same 2-t tip load, the maximum difference between the proposed 17-DOF model and the SimMechanics model was only 4.86% in the jib tip deflection. These results show that the proposed model can accurately represent the structural behavior of the crane while providing a computationally efficient reduced-order representation of the crane compared with detailed finite element modeling. The developed model provides a practical tool for structural analysis, vibration evaluation, design studies, and future control applications of real flat-top tower crane systems.

Keywords: flat top tower crane; finite element analysis; reduced-order modeling; discrete parameter system; modal analysis

1. Introduction

Tower cranes are among the most widely used lifting systems in modern construction projects due to their ability to transport heavy loads over large working areas and considerable heights. As the scale and complexity of construction projects continue to increase, the structural integrity, operational safety, and dynamic performance of tower cranes have become critical engineering concerns. During service, tower cranes are subjected to various static and dynamic loading conditions, including self-weight, payloads, wind actions, seismic excitations, and operational loads. These loading conditions may significantly influence the structural response, stability, and safety of the crane system [1–4].

Numerous studies have investigated the structural behavior of tower cranes using finite element methods. Gerdemeli et al. [5] performed finite element analyses to evaluate the structural performance of tower crane systems under operational loading conditions. Gu et al. [6] and Qing and Zeng [7] employed ANSYS-based numerical models to investigate stress distributions and deformation characteristics of tower crane structures. Karpe et al. [8] validated the applicability of finite element methods for both static and dynamic analyses of tower crane jibs. More recently, Zeng et al. [9] conducted stress and strain analyses of super-large tower crane connections and proposed parameter optimization strategies, whereas Zhang et al. [10] experimentally and numerically investigated the structural behavior of flat-top tower cranes under different working conditions. These studies demonstrated the effectiveness of finite element methods for assessing the structural safety and performance of tower crane systems.

In addition to static structural analyses, considerable attention has been devoted to the dynamic characteristics of tower cranes. Modal analysis is widely employed to determine natural frequencies and mode shapes, which are essential for evaluating resonance risks and vibration-related failures. Huang et al. [11] and Lei et al. [12] investigated the modal characteristics of tower crane structures using finite element techniques. Guo and Chen [13] examined the modal and fatigue behavior of critical crane components, while Trong et al. [14] performed modal analyses of damaged tower crane structures and validated their results experimentally. These studies highlighted the importance of accurately identifying the vibration characteristics of crane structures to ensure safe operation and structural reliability.

The influence of environmental and operational excitations on tower crane dynamics has also been extensively investigated. Wind-induced vibration responses were studied by Chen et al. [2], Jiang and Li [15], Jiang and Li [16], and Lu et al. [17], who demonstrated the significant effects of wind loading on crane safety and serviceability. Oliveira and Correia [18] compared the seismic and wind responses of tower crane systems, whereas Liu et al. [19] investigated vibration behavior under lifting–luffing coupled operating conditions. The findings of these studies emphasize the necessity of accurately characterizing the global dynamic behavior of tower cranes under realistic operating conditions.

Several researchers have proposed dynamic models to represent the behavior of tower crane systems. Rauscher and Sawodny [20] developed an elastic jib model for slewing control applications, while Stölzner et al. [21] investigated dynamic loads occurring during slewing operations. Furthermore, studies focusing on structural mechanics, joint behavior, and earthquake effects have contributed to the understanding of tower crane dynamics and structural performance [22–24]. Kenan and Azeloğlu [25] applied similitude theory to the design of a scaled tower crane mast model, and Zhu and Wang [26] performed static and modal analyses of crane arms using ANSYS. Hric et al. [27] additionally examined the structural characteristics of tower cranes from a truss-system perspective. More recently, Hou et al. [28] developed a nonlinear dynamic model of a tower crane considering friction and wind disturbances, demonstrating the applicability of advanced dynamic modeling techniques for improving crane performance under realistic operating conditions.

Although significant research has been conducted on the structural and dynamic behavior of tower cranes, most existing studies primarily focus on finite element analyses of complete structures or on specific structural components. The available literature does not report a validated 17-DOF reduced-order model developed directly from finite element-derived stiffness parameters for a real flat-top tower crane. Moreover, studies integrating finite element analysis, component-based modal characterization, reduced-order mathematical modeling, and elastic multibody validation within a unified framework remain limited.

Therefore, the present study aims to investigate the structural and dynamic behavior of a real 60/15 flat-top tower crane with a free-standing height of 48 m. Static analyses are performed to evaluate stress distributions and displacement responses of the main structural components. Modal analyses are subsequently conducted to determine the vibration characteristics of the crane substructures. In addition, a 17-DOF discrete mathematical model is developed using stiffness parameters derived from finite element analyses. The proposed model is validated through comparison with an elastic MATLAB/SimMechanics model under identical loading conditions. The developed framework provides a computationally efficient and physically representative approach for the structural assessment and dynamic evaluation of flat-top tower crane systems. Main contributions of this study are as follows:

A real 60/15 flat-top tower crane was comprehensively analyzed using finite element methods to determine its structural behavior, including stress, deformation, and modal characteristics.

A 17-degree-of-freedom reduced-order mathematical model was developed using stiffness parameters derived directly from finite element analyses and physical properties obtained from the computer-aided design (CAD) model.

The proposed reduced-order model was validated through comparison with an independently developed elastic multibody model in MATLAB/SimMechanics, demonstrating good agreement in structural response.

An integrated framework combining finite element analysis, reduced-order dynamic modeling, and elastic multibody simulation was established for the same real tower crane system, providing an efficient basis for future structural and control studies.

The remainder of this paper is organized as follows: Section 2 presents the finite element analyses and the development of the reduced-order mathematical model. Section 3 describes the elastic multibody model developed in MATLAB/SimMechanics for validation purposes. Section 4 presents and discusses the structural and dynamic analysis results. Finally, Section 5 summarizes the main conclusions and provides recommendations for future work.

2. Materials and methods

A flat-top tower crane was selected as the case study in the present investigation. Flat-top tower cranes have been widely employed in both single-building and large multi-building construction projects owing to their operational flexibility and structural advantages. Although they exhibit lifting characteristics similar to conventional hammerhead tower cranes, flat-top configurations have gained increasing popularity in recent years. The absence of a tower head simplifies assembly and dismantling procedures, reduces material and labor requirements, and facilitates the simultaneous operation of multiple cranes within congested construction sites. These advantages have contributed to the growing market share and widespread adoption of flat-top tower crane systems.

The tower crane considered in this study represents a real 60/15 flat top crane with a free-standing height of 48 m. A three-dimensional solid model of the crane was developed using SolidWorks software by considering the actual geometric characteristics and structural configuration of the system. The model included the principal load-carrying components of the crane, namely the mast sections, slewing platform, counter-jib, and jib assembly. The generated CAD model served as the basis for the subsequent finite element analyses and reduced-order dynamic modeling procedures.

The fundamental design specifications and lifting capacity characteristics of the investigated tower crane are summarized in **Table 1**. The three-dimensional model of the flat-top tower crane developed in SolidWorks is presented in **Figure 1**.

Table 1. Technical specifications of the flat-top tower crane.

Tower crane model	Maximum lifting capacity (kg)	Maximum tip load capacity (kg)	Free standing height (m)	Jib and counter jib length (m)
Flat Top	10.000	2,000	48	60–15

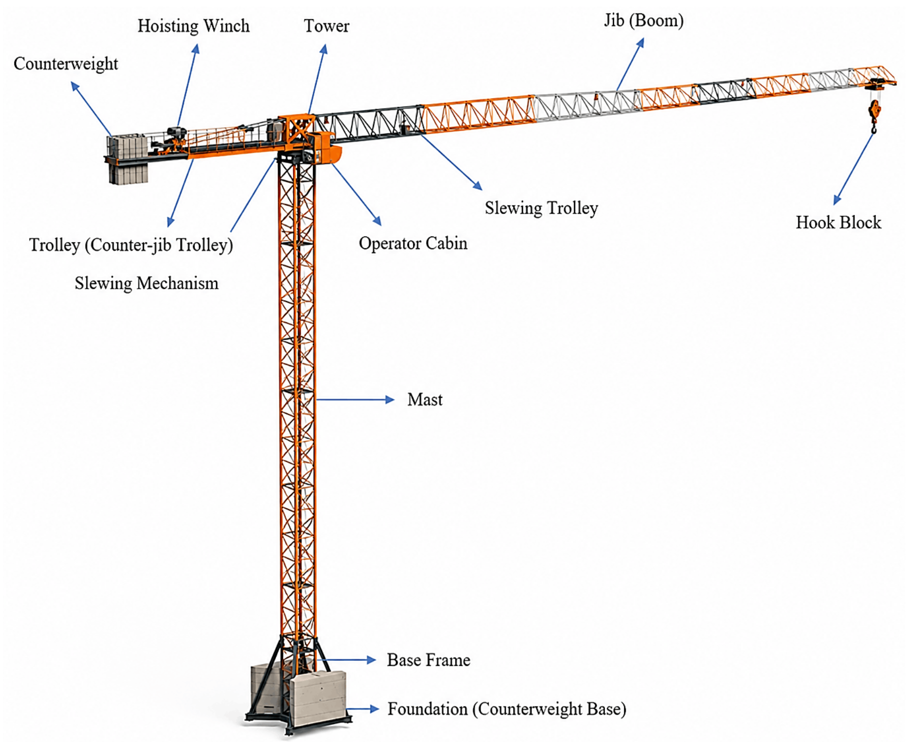

Figure 1. Three-dimensional design model of the investigated flat-top tower crane.

Static analyses of the investigated tower crane were performed using the ANSYS Workbench environment. Owing to the large dimensions of the crane and the complexity associated with modeling the entire structure using detailed finite elements, a full-scale solid analysis of the complete assembly was not considered computationally efficient. Therefore, the principal load-carrying components of the crane, including the base frame, mast, tower, jib, and counter-jib, were analyzed individually by applying appropriate remote loading conditions representing the actual operational loads transferred between structural members.

Accurate material characterization is essential for reliable finite element simulations and proper interpretation of the obtained results. The mechanical properties of the structural steel directly influence the predicted stress distributions, deformation responses, and overall structural performance of the crane system. Nevertheless, the evaluation of structural safety cannot be based solely on material properties. Design considerations should also account for potential failure mechanisms such as yielding, instability, fatigue damage, and brittle fracture.

Adequate structural safety in steel constructions requires the selection of appropriate material grades together with suitable safety factors corresponding to the expected service conditions. The safety factors employed in the design and assessment of tower cranes are explicitly defined in the FEM 1.001 standard. In addition, the manufacturing quality of steel structures significantly influences the selection of these factors. In particular, weld configuration and weld quality affect the fatigue strength and load-carrying capacity of structural members. According to FEM 1.001, welded details are classified into three categories based on their manufacturing characteristics, as illustrated in **Figure 2**.

- Category I, members without welds or with transverse welds;
- Category II, members containing longitudinal welds;
- Category III, welded joint regions.

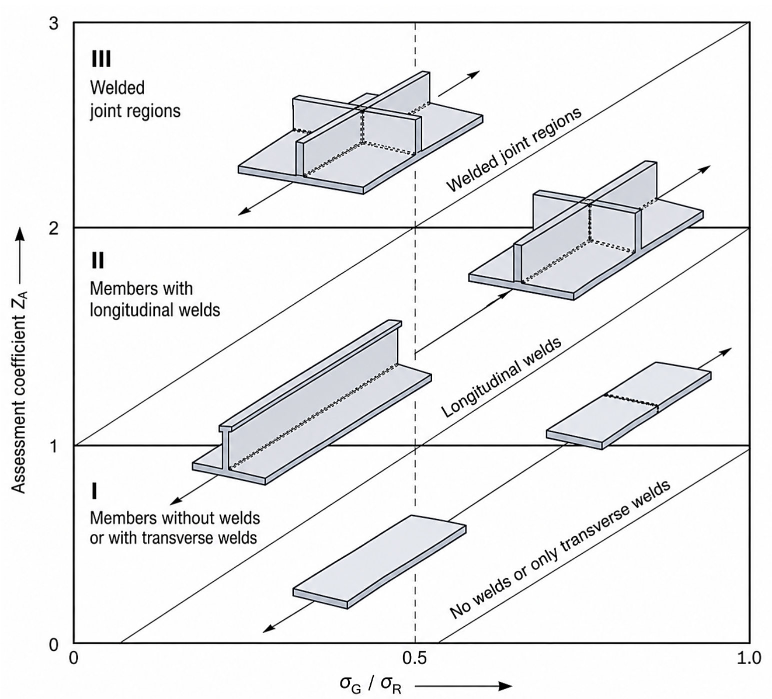

Figure 2. Classification of welded structural details according to FEM 1.001.

For members subjected to relatively low stress levels, Category I values may also be adopted for all weld types when post-weld stress-relief heat treatment is applied at approximately 600–650 °C. The safety factors and the corresponding design recommendations adopted in this study according to FEM 1.001 are summarized in **Table 2**.

Table 2. Allowable stresses for different steel grades according to FEM 1.001.

Steel grade	Yield strength (N/mm^2)	Allowable stress (N/mm^2) Category I	Allowable stress (N/mm^2) Category II	Allowable stress (N/mm^2) Category III
E.24 (A.37, Fe 360)	240	160	180	215
E.26 (A.42)	260	175	195	240
E.24 (A.52, Fe 510)	360	240	270	325

The structural components of the investigated tower crane were assumed to be manufactured from S355J0 structural steel (St-52). According to the FEM 1.001 standard, the equivalent material grade of S355J0 corresponds to A.52. Based on the classification of welded structural details presented previously, Category I was adopted for the assessment of allowable stresses. Consequently, an allowable stress value of 240 MPa was considered as the acceptance criterion for evaluating the finite element analysis results. Therefore, stress values obtained from the numerical analyses lower than this limit were regarded as satisfactory in terms of structural safety.

2.1. Modal analysis

Modal analysis is a fundamental technique used to determine the natural frequencies and corresponding mode shapes of a structure. The natural frequency represents the frequency at which a structure vibrates freely in the absence of external excitation and is governed primarily by the mass and stiffness characteristics of the system. When an external excitation contains frequency components close to the natural frequencies of the structure, resonance may occur, resulting in a substantial increase in vibration amplitudes that can adversely affect structural integrity and operational safety.

Mode shapes describe the deformation patterns associated with each natural frequency and provide valuable insight into the dynamic behavior of the structure. For unconstrained systems, the first six vibration modes are theoretically expected to correspond to rigid-body motions, involving translational and rotational movements along and about the three principal axes without structural deformation. Beginning from the seventh mode, the structure exhibits elastic deformation, and the corresponding mode shapes represent the actual vibration characteristics of the system.

The identification of natural frequencies and mode shapes enables engineers to improve both the safety and the efficiency of structural systems. Tower cranes, owing to their slender and flexible configurations, are particularly susceptible to dynamic effects. External excitations, especially low-frequency wind loads, may significantly influence their vibration behavior. Therefore, evaluating only the static response of tower cranes is insufficient for a comprehensive structural assessment. The dynamic characteristics of the structure should also be identified to determine whether resonance-related problems may arise and to establish appropriate design modifications or optimization strategies when necessary. The critical load-carrying components of the investigated flat-top tower crane were analyzed using the ANSYS Workbench environment to determine their natural frequencies and mode shapes. The obtained natural frequencies and mode shapes were subsequently utilized to assess the vibration characteristics and dynamic performance of the crane structure.

2.2. Reduced order system and mathematical modeling

Recent studies have also emphasized the importance of reduced-order multibody formulations for tower crane dynamic analysis and computational efficiency [29]. Complex physical systems generally exhibit continuous, multi-component, and spatially distributed dynamic behavior. Such systems are commonly described by partial differential equations, and obtaining analytical solutions is often difficult or impractical. Discrete system modeling provides an effective approach for simplifying these complex systems, enabling numerical analyses and facilitating subsequent dynamic investigations. In this approach, a continuous physical system is idealized using a finite number of discrete elements, such as masses, springs, and dampers, thereby yielding a simplified yet representative model that preserves the dominant characteristics of the original structure.

In the present study, the actual flat-top tower crane was represented as a discrete system to capture its global dynamic behavior with reduced computational effort. The proposed reduced-order model of the crane is illustrated in **Figure 3**. Based on the adopted discretization scheme, the equations of motion associated with each component were derived using Newton's second law of motion.

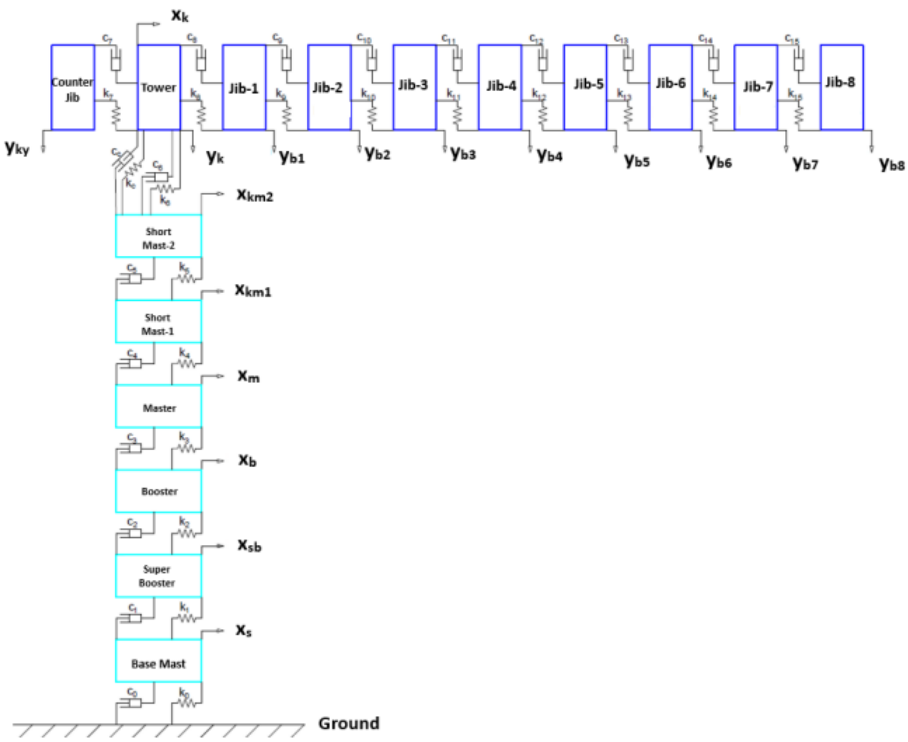

Figure 3. Seventeen-degree-of-freedom (17-DOF) discrete parameter model of the investigated 60/15 flat-top tower crane.

The equations of motion establish the relationship between the dynamic variables of a physical system, such as displacement, velocity, and acceleration, and the external forces acting on the system. These equations provide the mathematical framework required to describe the dynamic response of the structure and enable both analytical and numerical investigations. Since the developed discrete representation constitutes a multi-degree-of-freedom (MDOF) system, the governing equations of motion can be expressed in matrix form as

$$M\ddot{q} + C\dot{q} + Kq = F(t) \tag{1}$$

where *M*, *C*, and *K* denote the mass, damping, and stiffness matrices of the system, respectively; $q(t)$ represents the generalized displacement vector associated with the degree of freedom; and $F(t)$ corresponds to the vector of time-dependent external excitations.

The developed reduced-order formulation consists of a total of seventeen degrees of freedom. In the adopted coordinate system, the base frame, mast, and tower components were assumed to undergo translational motion in the horizontal (x) direction, whereas the counter-jib, tower–trolley assembly, and jib components were allowed to move in the vertical (y) direction. The tower trolley assembly possesses both horizontal and vertical translational motions and therefore constitutes the coupling element of the system. To ensure compatibility between the horizontal and vertical dynamic responses and to represent the interaction between these motions, an additional coupling spring (k_c) and damping element (c_c) were introduced into the discrete model. Consequently, the proposed 17-DOF model enables the integrated dynamic assessment of the entire crane structure while maintaining a computationally efficient formulation.

Figure 3 illustrates the proposed 17-DOF discrete model developed to represent the global dynamic behavior of the investigated flat-top tower crane. The actual crane structure was idealized as an interconnected discrete parameter system composed of concentrated masses, equivalent springs, and viscous dampers. The model was established by considering the dominant deformation regions and the principal load-carrying components of the crane.

The mast system was represented by six horizontal translational degrees of freedom, namely the base mast (x_s), super booster (x_{sb}), booster (x_b), master mast (x_m), short mast-1 (x_{km1}), and short mast-2 (x_{km2}). These components were interconnected through equivalent stiffness and damping elements (k_0–k_6) and (c_0–c_6), thereby capturing the lateral flexibility of the tower structure.

The upper assembly of the crane consisted of the counter-jib, tower, and jib sections. The counter-jib and the jib segments were assumed to undergo vertical translational motions represented by the generalized coordinates (y_{ky}), (y_{b1}), (y_{b2}), …, (y_{b8}). The tower component, denoted by (y_k), served as the transition region between the mast and jib assemblies. Equivalent spring and damping elements (k_7–k_{15}) and (c_7–c_{15}) were introduced to model the elastic interactions between adjacent components.

Since the tower component experiences both horizontal and vertical dynamic interactions, an additional coupling spring (k_c) and damping element (c_c) were incorporated into the formulation to establish compatibility between the mast and upper structural assemblies. This coupling mechanism enables the simultaneous representation of horizontal and vertical vibration characteristics within a unified mathematical framework.

The resulting 17-DOF discrete parameter model preserves the dominant dynamic characteristics of the actual crane structure while substantially reducing computational complexity. Consequently, the proposed formulation provides an efficient platform for dynamic analyses and subsequent validation studies through comparison with the elastic multibody model developed in MATLAB/SimMechanics.

The discrete representation of the flat-top tower crane system was introduced in **Figure 3**. To derive the governing equations of motion, each structural component was subsequently modeled as an individual subsystem. **Figure 4** presents the free-body diagram of the booster mast segment used for the derivation of the equations of motion. Equivalent subsystem models were established for all remaining components, enabling the formulation of the complete multi-degree-of-freedom dynamic model of the tower crane. Equations of motion corresponding to the 17-DOF discrete model are included in **Appendix A**.

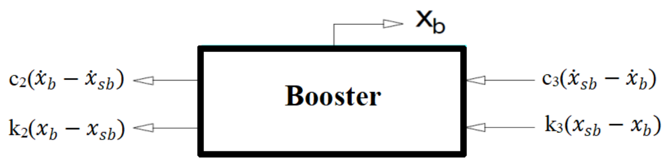

Figure 4. Free-body diagram representation of the third mast (booster).

The mass, stiffness, and damping parameters required for the formulation of the reduced-order model were subsequently determined. The mass values incorporated into the model were obtained directly from the three-dimensional CAD model developed in SolidWorks. Following the assignment of the corresponding material properties, the mass of each structural component was extracted individually and introduced into the discrete parameter representation. For the finite element analyses, a vertical concentrated load corresponding to the maximum rated tip load of the crane (2 t) was applied at the free end of the jib. The base frame of the crane was fully constrained to represent the actual support conditions. For the remaining structural components, equivalent remote loads representing the actual load transfer during crane operation were applied. The resulting displacement values obtained from these analyses were subsequently used to calculate the equivalent stiffness coefficients according to Hooke's law.

The stiffness coefficient is a fundamental engineering parameter that quantifies the resistance of a structural member or mechanical component against elastic deformation. This parameter is directly related to the displacement generated under an applied load and, for linear elastic systems, is commonly described by Hooke's law. Accordingly, the force–displacement relationship may be expressed as

$$F = kx \quad (2)$$

where F denotes the applied force (N), x represents the resulting displacement (m), and k is the stiffness coefficient (N/m).

In the present study, the equivalent stiffness coefficients of the crane components were determined using deformation data obtained from the finite element analyses conducted in ANSYS Workbench. Appropriate remote loads representing the actual load transfer conditions were applied to the structural members, and the resulting displacement responses were extracted from the numerical simulations. The equivalent stiffness values were subsequently calculated from the force-displacement relationship according to Hooke's law. This procedure enabled the distributed flexibility of the actual crane structure to be represented by equivalent spring elements within the 17-DOF discrete formulation.

A structural member subjected to bending deformation may be represented by an equivalent mass–spring system. The idealized model adopted for the determination of the equivalent stiffness parameters is illustrated in **Figure 5**. The damping coefficients employed in the reduced-order model were determined analytically and incorporated into the governing equations of motion to account for the energy dissipation characteristics of the structural system.

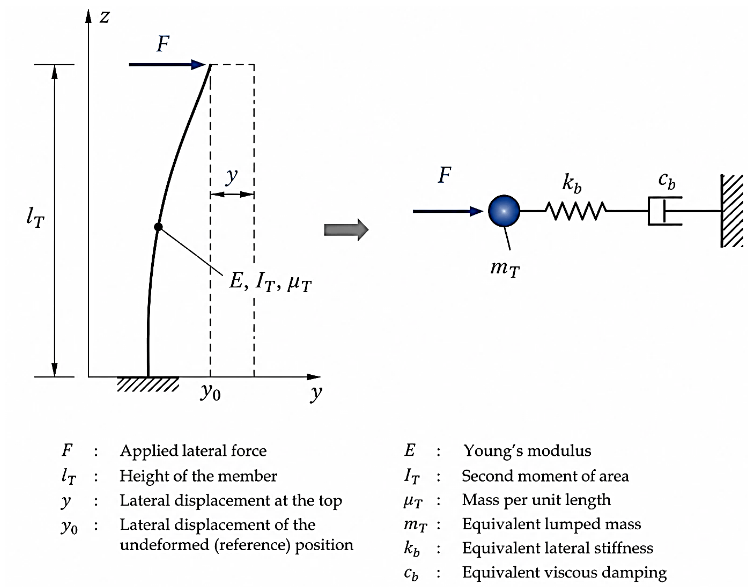

Figure 5. Idealized mass–spring–damper representation of an elastic tower under bending vibrations, redrawn based on Rauscher and Sawodny [20].

Structural members possessing simple geometrical configurations allow the equivalent stiffness coefficients to be determined directly from their cross-sectional and mechanical properties. The corresponding formulation is presented in Equation (3).

$$F = kx = \frac{3EI}{L^3} \tag{3}$$

Analytical determination of the equivalent stiffness coefficients was not feasible because of the truss-type structural configuration and the geometric complexity of the investigated flat-top tower crane. Therefore, the stiffness values were obtained through finite element analyses performed using the ANSYS Workbench environment. Appropriate external forces were applied to the free ends of the structural components, and the resulting displacements in the loading directions were extracted from the numerical simulations. The equivalent stiffness coefficients were subsequently calculated by substituting the corresponding force and displacement values into the force–displacement relationship defined by Hooke's law.

The damping coefficient (c) is a fundamental parameter that quantifies the energy dissipation characteristics of a mechanical system and governs the decay of vibration amplitudes with time. Damping arises from mechanisms such as friction, viscous effects, and intrinsic material losses, through which vibration energy is gradually transformed into heat or other forms of energy. Physically, the damping coefficient represents the damping force generated per unit velocity and is commonly expressed as

$$F = c\dot{x} \tag{4}$$

where F is the damping force (N), c is the damping coefficient (N·s/m), and $\dot{x}$ is the velocity (m/s).

Determination of damping coefficients is generally based either on experimentally identified damping ratios or on damping values recommended by design standards. Since the investigated crane system remained at the design stage and experimental measurements were unavailable, the damping coefficients adopted in this study were estimated using damping ratios selected from the relevant standards. The damping coefficient was calculated according to

$$c = 2\zeta\sqrt{km} \tag{5}$$

where ζ is the damping ratio, k is the equivalent stiffness coefficient (N/m), and m is the equivalent discrete mass (kg).

Selection of the damping ratio was based on the recommendations reported by Kenan and Azeloğlu [25]. Considering that tower cranes generally operate under stress levels well below the yielding limit during normal service conditions and consist predominantly of welded steel structural members, damping ratios ranging between 2% and 3% have been suggested to adequately represent their energy dissipation characteristics. Accordingly, a damping ratio was adopted in the present study. The damping coefficients of all structural components were subsequently calculated individually using the corresponding equivalent mass and stiffness values.

The mass, stiffness, and damping matrices obtained from the developed equations of motion are provided in **Appendix B**, whereas the numerical values of the calculated M, K, and C matrices are presented in **Appendix C**. These matrices constitute the mathematical basis of the proposed 17-DOF reduced-order model and were employed in the subsequent dynamic analyses and validation studies.

2.3. Development of the elastic multibody model

An alternative modeling approach was employed to investigate the dynamic behavior of the investigated flat-top tower crane and to provide an independent basis for validating the proposed reduced-order formulation. An elastic multibody model of the crane was developed using SolidWorks and MATLAB/Simulink/Simscape Multibody. The primary objective of adopting this modeling technique was to evaluate the influence of the actual mass and inertia properties of the structural components on the dynamic response of the system under operational loading conditions. According to the literature, multibody modeling techniques enable the dynamic analysis of complex mechanical systems without the explicit derivation of detailed mathematical formulations. Furthermore, such approaches preserve the physical characteristics of the structure while providing a realistic representation of the interactions between individual components. Similar flexible multibody formulations have recently been employed for tower crane dynamic simulations to improve the representation of structural flexibility while maintaining computational efficiency [30].

Initially, three-dimensional solid models of the principal structural components of the flat-top tower crane, including the base frame, mast system, tower assembly, and jib structure, were generated in SolidWorks using their actual dimensions. Material properties were subsequently assigned to each component, allowing their corresponding mass and inertia characteristics to be calculated automatically. Following the completion of the assembly process, the SolidWorks model was exported to the MATLAB environment to establish an elastic multibody formulation. The overall procedure adopted for the dynamic modeling process using SolidWorks and MATLAB is illustrated in **Figure 6**.

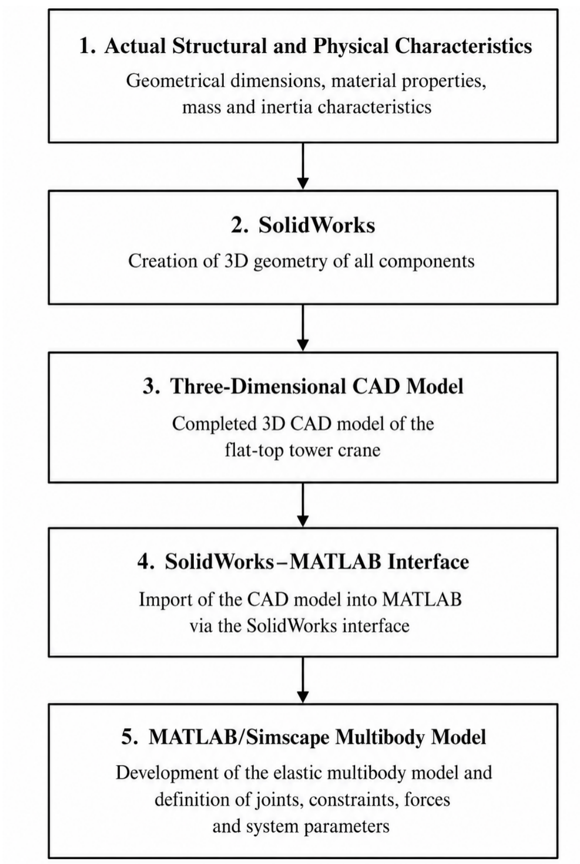

Figure 6. Workflow adopted for the development of the elastic multibody model of the investigated flat-top tower crane.

The simulation model developed in MATLAB/Simscape Multibody is presented in **Figure 7**. For the sake of clarity, only the subsystem representations of the base frame, mast, and tower assemblies are shown. Equivalent stiffness and damping elements, represented by the coefficients (K) and (C), were incorporated into each subsystem and defined along the corresponding Cartesian directions to account for structural flexibility.

These parameters were obtained from the finite element analyses performed in ANSYS Workbench, as described in the previous sections.

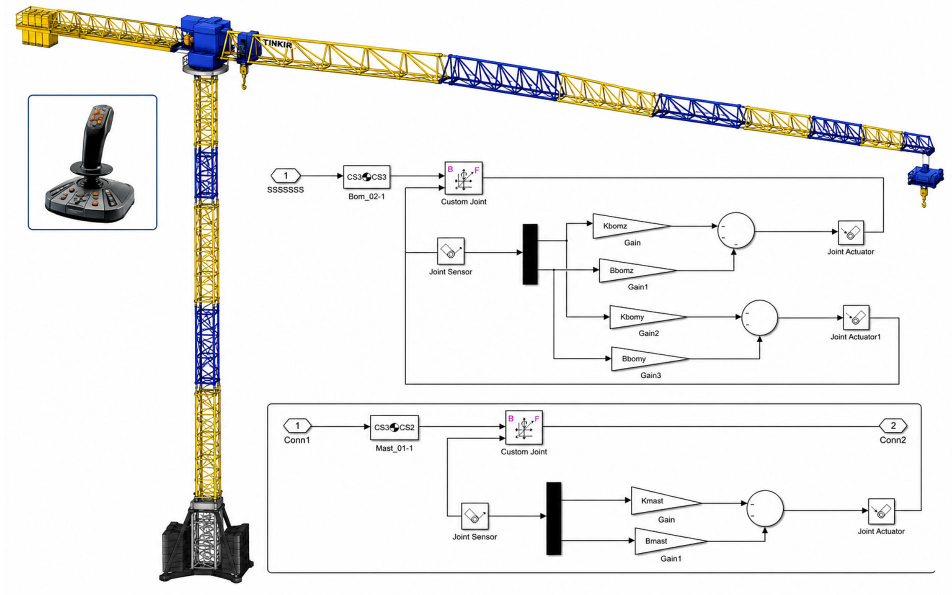

Figure 7. Elastic MATLAB/SimMechanics simulation model of the investigated flat top tower crane.

In addition to the elastic deformation characteristics, the slewing motion of the tower crane was incorporated into the multibody formulation by allowing rotational motion about the global y-axis. Consequently, the developed elastic multibody model preserves the actual mass and inertia properties of the crane components while incorporating the flexibility characteristics identified through finite element analyses. The resulting formulation provides a realistic representation of the structural dynamics of the crane and serves as a reference model for validating the proposed 17-DOF reduced-order mathematical model. Representative views of the elastic tower crane model developed in MATLAB/Simscape Multibody are presented in **Figure 8**.

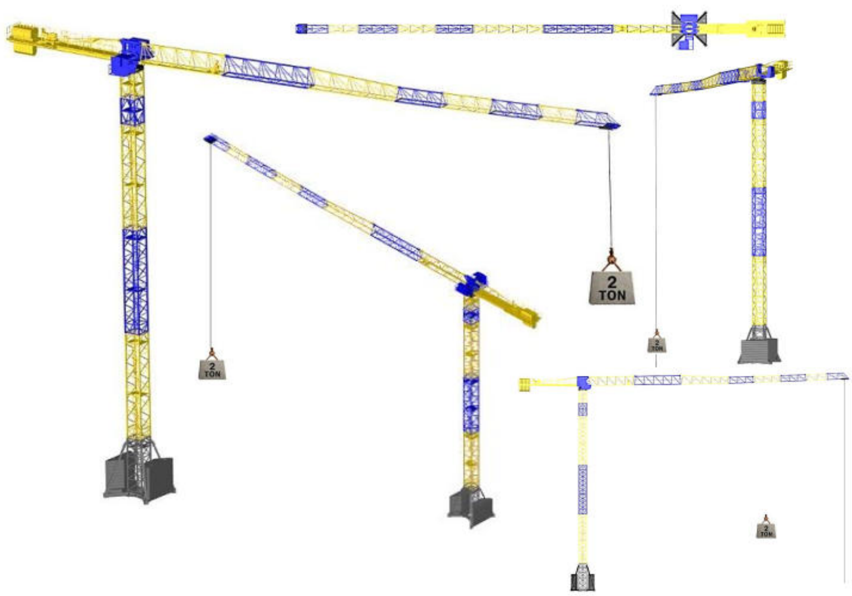

Figure 8. Representative views of the elastic MATLAB/SimMechanics model of the investigated flat top tower crane.

3. Results

The results obtained from the finite element analyses, reduced-order modeling, and elastic multibody simulations are presented and discussed in this section. First, the structural performance of the investigated flat-top tower crane is evaluated through static analyses by examining the stress distributions and displacement responses of the principal load-carrying components under the prescribed loading conditions. Subsequently, the dynamic characteristics of the crane are investigated through modal analyses to identify the natural frequencies and corresponding mode shapes of the structure. Finally, the predictive capability of the proposed 17-DOF reduced-order model is assessed through comparison with the elastic MATLAB/SimMechanics model. The obtained results provide a comprehensive understanding of the structural integrity and dynamic behavior of the actual tower crane system and demonstrate the applicability of the proposed modeling framework for structural assessment and future design optimization studies.

3.1. Structural analysis results

Static structural analyses were performed in the ANSYS Workbench environment by applying remote loads corresponding to the actual operating conditions of the investigated flat-top tower crane. The applied loads included the self-weight of the structural components, counterweights, and the maximum rated payload acting at the tip of the jib.

The analyses were conducted under the most critical loading condition corresponding to the maximum lifting capacity. For the base frame, the maximum equivalent (von Mises) stress was determined to be 140.89 MPa. This value remained well below the allowable stress limit of 240 MPa specified for Category I welded steel structures according to the FEM 1.001 standard, indicating that the base frame satisfies the structural safety requirements under the investigated loading conditions.

The maximum displacement of the base frame was found to be 2.4 mm. For structural members fixed at both ends, the allowable deflection limit is commonly taken as (L/1,000), where (L) represents the span length. Considering that the total length of the base frame is 6,000 mm, the corresponding allowable displacement limit was calculated as 6 mm. Since the obtained displacement value was substantially lower than this limit, the base frame can be regarded as structurally adequate in terms of serviceability requirements.

The stress distribution and displacement contours obtained from the finite element analyses of the base frame are presented in **Figure 9**.

The results demonstrate that the investigated base frame exhibits sufficient strength and stiffness to safely withstand the prescribed loading conditions. Although the mast assembly consists of five individual segments, its static structural behavior was evaluated by considering the mast as an integral structural component. Accordingly, remote loads representing the actual operating conditions were applied to the complete mast assembly, and the finite element analysis was performed on the assembled structure as a whole. This approach enabled the load transfer mechanisms and the interaction between the individual mast segments to be adequately represented, thereby providing a realistic assessment of the overall stress distribution and deformation characteristics of the mast system.

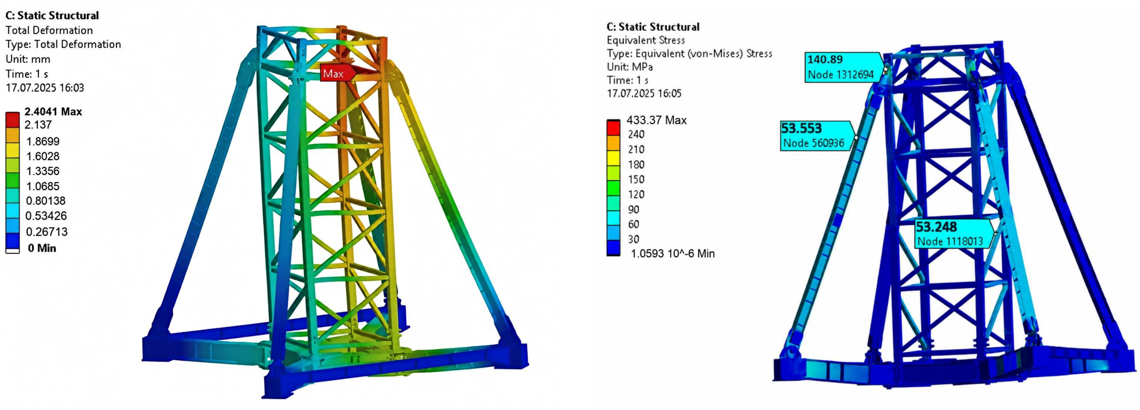

(a) (b)

Figure 9. Structural analysis of the base frame: **(a)** Total deformation distribution; **(b)** Equivalent (von Mises) stress distribution.

The static analysis results of the mast indicated that the maximum equivalent (von Mises) stress reached 102.26 MPa, whereas the maximum displacement was determined to be 183.94 mm. The obtained stress value remained considerably lower than the allowable stress limit of 240 MPa specified for Category I welded steel structures according to the FEM 1.001 standard, demonstrating that the mast satisfies the required strength criteria under the investigated loading conditions. The maximum lateral deflection of the mast was calculated as 183.94 mm. According to the AISC 360 specification, the allowable deflection limit for cantilever structural members may be taken as (L/180), where (L) denotes the member length. Since the mast was designed with a total height of 40,900 mm, the corresponding allowable deflection limit was calculated as 227.22 mm. The predicted deflection remained below this threshold, indicating that the mast also satisfies the serviceability requirements in terms of structural stiffness.

The stress and deformation contours obtained from the finite element analyses are presented in **Figure 10**. The results demonstrate that the mast possesses sufficient strength and rigidity to safely sustain the prescribed loading conditions without exceeding the allowable stress and deflection limits.

According to the finite element analysis results obtained for the counter-jib assembly, the maximum displacement occurred at the free end of the counter-jib and was determined to be 20.2 mm. Considering the overall length and structural configuration of the component, the calculated displacement remained within the acceptable serviceability limits, indicating that the counter-jib possesses sufficient stiffness under the investigated loading conditions.

The maximum equivalent (von Mises) stress was observed in the counter-jib tie members, where the highest stress value reached 220.82 MPa. This value remained below the allowable stress limit of 240 MPa specified for Category I welded steel structures according to the FEM 1.001 standard. Therefore, the stress level can be considered acceptable, and the structural integrity of the counter-jib assembly is maintained under the maximum loading condition.

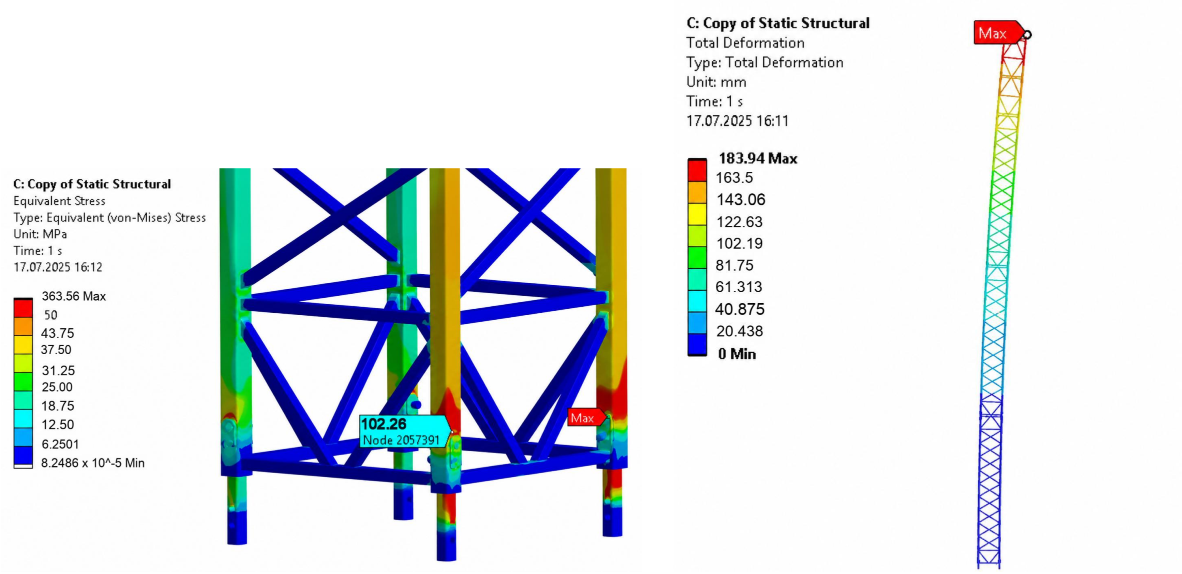

(a) **(b)**

Figure 10. Mast structural analysis: **(a)** Mast equivalent stress result; **(b)** Mast total deformation result.

The maximum displacement at the counter-jib tip and the stress concentration regions occurring in the counter-jib and tie members are illustrated in **Figure 11**. The results obtained demonstrate that the counter-jib assembly satisfies both the strength and serviceability requirements of the design.

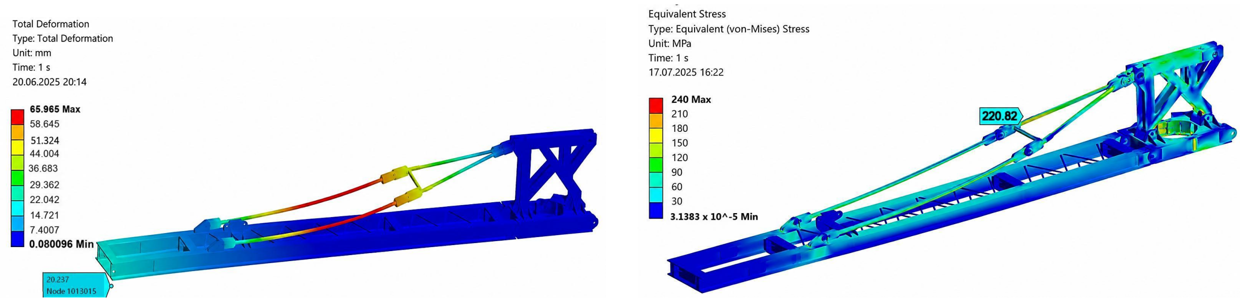

(a) **(b)**

Figure 11. Counter-jib structural analysis: **(a)** Counter-jib total deformation result; **(b)** Counter-jib equivalent stress result.

The finite element analysis results indicated that the maximum displacement occurred at the tip of the jib and reached 1,490 mm. This displacement value was found to be nearly equal to the predefined reverse camber introduced during the design stage, demonstrating that the intended deformation compensation was successfully achieved under the maximum loading condition. Consequently, the resulting deflection remained within the acceptable operational limits, indicating that the jib structure satisfies the serviceability requirements.

The stress analysis revealed that the highest stress concentrations occurred in the first and sixth jib segments. The maximum equivalent (von Mises) stress obtained from the analysis was 225 MPa. This value remained below the allowable stress limit of 240 MPa specified for Category I welded steel structures according to the FEM 1.001 standard. Therefore, the jib structure can be considered structurally safe with respect to strength requirements under the investigated loading condition.

The stress distributions and deformation obtained from the finite element analyses are presented in **Figure 12**. The results confirm that the jib structure satisfies both the strength and serviceability criteria and is capable of safely carrying the prescribed maximum payload.

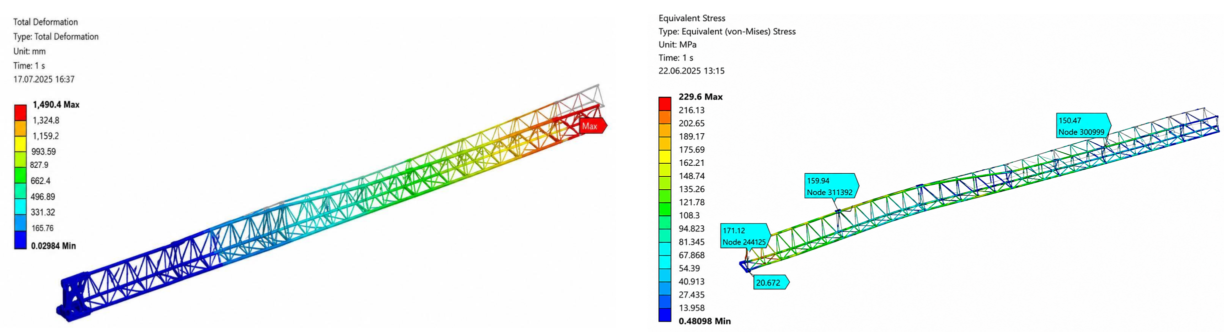

(a) **(b)**

Figure 12. Jib structural analysis: **(a)** Jib total deformation result; **(b)** Jib equivalent stress result.

The static analysis results indicated that the tower–slewing platform assembly experienced an approximately 7 mm displacement toward the jib side under the maximum loading condition. This behavior demonstrates that the structure tends to deflect in the direction of the applied load. Considering the operational characteristics of tower cranes, the maximum bending moment is expected to occur toward the jib side when the crane is subjected to payload loading. The deformation pattern observed in the tower–slewing platform assembly is therefore consistent with the mast deflection direction identified in the previous analyses. The agreement between these independent structural responses further supports the reliability and accuracy of the finite element model.

The stress analysis revealed that the highest stress concentrations occurred in the pin connection regions, where the maximum equivalent (von Mises) stress reached 219.45 MPa. In contrast, the stress levels observed in the plate elements forming the main body of the structure generally ranged between 100 and 150 MPa. Although all stress values remained below the allowable stress limit of 240 MPa specified by the FEM 1.001 standard for Category I welded steel structures, several regions exhibited relatively low stress utilization. Consequently, topology optimization studies may be considered for these areas to achieve further weight reduction without compromising structural integrity.

The stress distributions and total deformation obtained from the finite element analyses are presented in **Figure 13**. The results confirm that the tower–slewing platform assembly satisfies the required strength and serviceability criteria while also indicating potential opportunities for structural optimization.

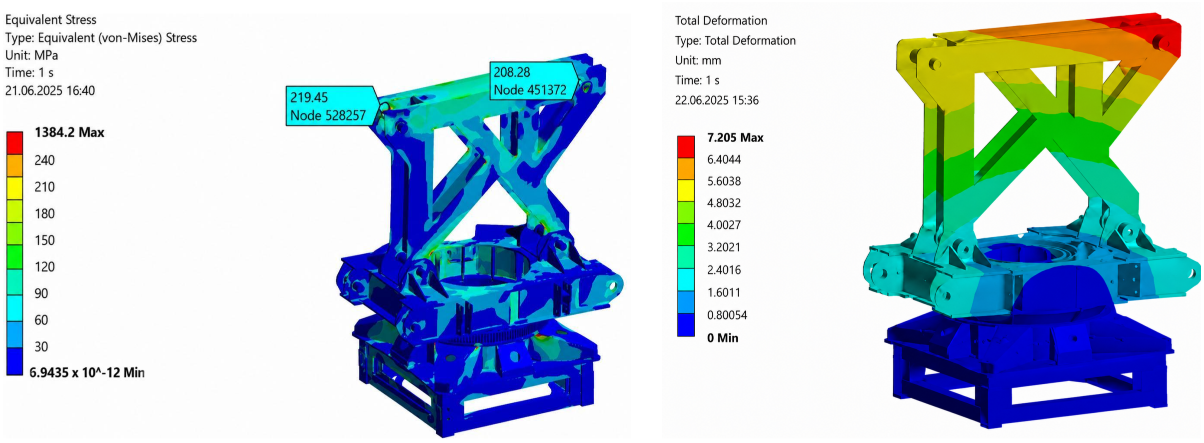

(a) **(b)**

Figure 13. Tower–slewing platform structural analysis: **(a)** Tower–slewing platform stress result; **(b)** Tower–slewing platform deformation result.

A summary of the maximum stress and displacement values obtained for all structural components investigated in this study is presented in **Table 3**. The results indicate that all components satisfy the allowable stress and serviceability requirements specified by the applicable design criteria. Furthermore, the comparison of stress and deformation responses enables the identification of the most critical structural members and provides valuable information for future optimization and design improvement studies.

Table 3. Summary of the maximum displacement and equivalent stress results obtained for the main structural components of the tower crane.

Component	Maximum displacement (mm)	Maximum equivalent stress (MPa)
Base Frame	2.4	140.89
Mast	184	102
Counter-Jib	20.2	220.82
Jib	1,490	225
Tower–Slewing Platform	7.37	219.45

The stress distributions indicate that the highest stresses occur near the connection regions, where load transfer between the structural members is concentrated. Nevertheless, all stress values remain below the allowable limit, confirming the adequacy of the current structural design.

3.2. Modal analysis results

The modal characteristics of the tower crane were investigated by performing modal analyses on the individual structural components rather than on the complete crane assembly. This approach enabled the dynamic behavior and vibration characteristics of each load-carrying component to be evaluated independently. For each component, the natural frequencies and corresponding mode shapes were determined under free vibration conditions.

Accordingly, the first six vibration modes were examined to verify the existence of rigid-body motions associated with unconstrained structures. Following confirmation of these modes, the seventh mode was considered the first critical deformation mode and was therefore selected for detailed evaluation. Since the seventh mode represents the onset of structural deformation, it provides valuable information regarding the dynamic behavior and vibration sensitivity of the corresponding component.

A total of twelve vibration modes were extracted and analyzed for each structural component. The modal analyses were performed for the base frame, long mast, short mast, counter-jib, tower–slewing platform assembly, and the eight jib segments. To provide a representative comparison of the dynamic characteristics of these components, only the first critical deformation mode (Mode 7) is presented and discussed in this study.

The Mode 7 deformation patterns obtained from the modal analyses of the base frame, long mast, short mast, jib segments (Jib-1–Jib-8), counter-jib, and tower–slewing platform assembly are presented in **Figure 14**, respectively. These results provide insight into the dominant vibration characteristics of the individual structural components and identify the regions most susceptible to dynamic deformation.

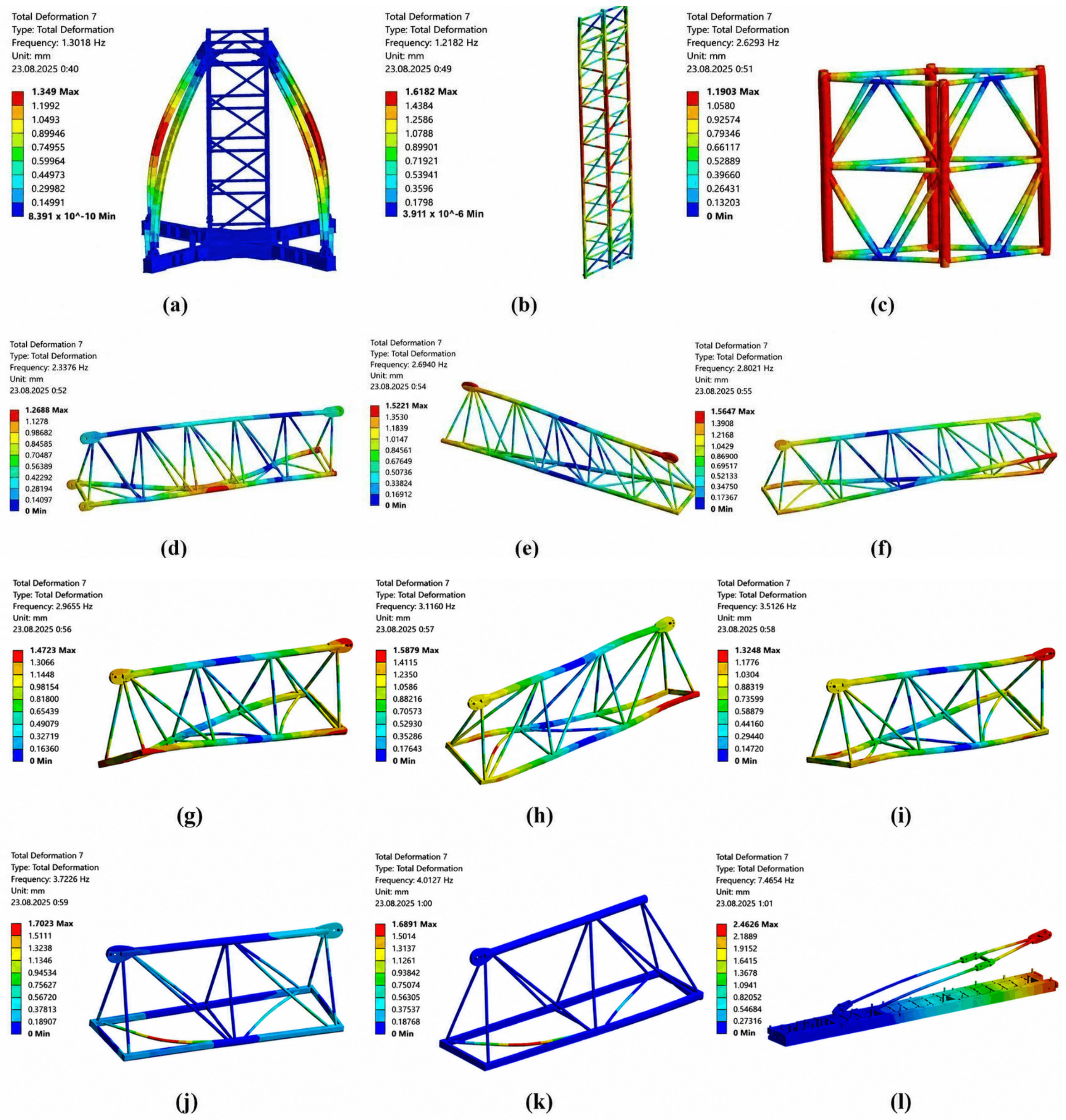

Figure 14. *Cont.*

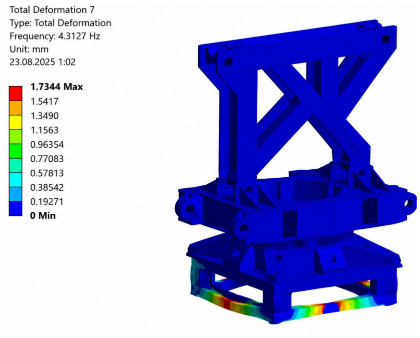

(m)

Figure 14. Mode 7 deformation patterns of the investigated tower crane subcomponents obtained from free–free modal analysis: **(a)** Base frame; **(b)** Long mast; **(c)** Short mast; **(d)** Jib-1; **(e)** Jib-2; **(f)** Jib-3; **(g)** Jib-4; **(h)** Jib-5; **(i)** Jib-6; **(j)** Jib-7; **(k)** Jib-8; **(l)** Counter-jib; **(m)** Tower–slewing platform assembly.

The modal analyses of all subcomponents constituting the main structural elements of the tower crane were performed individually using ANSYS. In order to determine the intrinsic vibration characteristics of each component, free–free modal analyses were conducted without imposing boundary constraints. This approach enabled the natural frequencies and mode shapes of the components to be evaluated independently of external support conditions.

Analysis results showed that the first six vibration modes of all investigated subcomponents were either zero or negligibly small. These modes correspond to rigid-body motions and therefore do not involve elastic deformation. Instead, they represent translational and rotational movements of the structure along and about the three Cartesian axes (x, y, and z). Since elastic deformation begins to occur from the seventh mode onward, the seventh mode was considered the first significant structural vibration mode, and its corresponding natural frequency was adopted as the first critical natural frequency of the component.

The modal analysis results demonstrated that the investigated structural components possess sufficient stiffness and exhibit natural frequencies that are generally outside the range associated with critical resonance conditions. Consequently, the dynamic characteristics of the majority of the components can be considered satisfactory from a vibration and structural integrity perspective. However, the counter-jib assembly exhibited a relatively low first deformation-mode frequency (Mode 7) due to the flexibility introduced by the tie members. This result indicates that the dynamic stiffness of the counter-jib may be insufficient under certain operating conditions. Therefore, additional structural optimization studies aimed at increasing the rigidity of this component are recommended.

The natural frequencies obtained from the modal analyses are summarized in **Table 4**. The natural frequencies presented in **Table 4** indicate that the investigated crane components exhibit different dynamic characteristics depending on their geometric configurations and stiffness properties. In general, components with higher natural frequencies possess greater structural stiffness, whereas lower frequencies are associated with relatively flexible structural behavior. The obtained results demonstrate that most of the investigated components provide sufficient dynamic stiffness and are unlikely to experience resonance under normal operating conditions. However, the counter-jib exhibited the lowest first elastic natural frequency among the analyzed components, indicating a greater sensitivity to dynamic excitation. This behavior can be attributed to the relatively slender structural configuration and the flexibility introduced by the tie members. Therefore, increasing the stiffness of the counter-jib structure may further improve its dynamic performance and vibration resistance.

Table 4. Summary of the natural frequencies obtained from the modal analyses.

Component	Rigid-body mode frequency (Hz)	Mode 7 frequency (Hz)	Mode 12 frequency (Hz)
Base Frame	1.44×10^{-3}	14.318	19.395
Long Mast	2.37×10^{-4}	17.334	48.919
Short Mast	4.30×10^{-3}	19.744	94.466
Jib-1	8.40×10^{-4}	16.796	53.132
Jib-2	3.29×10^{-2}	17.758	46.578
Jib-3	5.61×10^{-4}	18.173	43.277
Jib-4	4.92×10^{-3}	33.667	64.494
Jib-5	5.68×10^{-3}	35.113	60.837
Jib-6	4.16×10^{-3}	36.902	58.696
Jib-7	6.45×10^{-3}	34.807	41.037
Jib-8	5.58×10^{-3}	32.41	38.265
Counter-Jib	6.95×10^{-4}	0.64096	7.9367
Tower–Slewing	5.61×10^{-4}	34.497	61.566

The relatively low natural frequency of the counter-jib suggests that this component is more susceptible to dynamic excitation than the remaining structural members. Therefore, it should receive particular attention during the design and dynamic assessment of flat-top tower cranes.

3.3. Comparative analysis of the 17-DOF and SimMechanics models

The accuracy of the proposed 17-DOF discrete model was evaluated through comparison with the elastic MATLAB/SimMechanics model under identical loading conditions. A concentrated load of 2 t was applied at the jib tip in both models, and the resulting tip deflections were recorded. The obtained responses were subsequently compared to determine the predictive capability of the reduced-order model and to assess its suitability for representing the global structural behavior of the tower crane system.

As illustrated in **Figure 15**, the maximum jib tip deflection predicted by the elastic MATLAB/SimMechanics model was approximately 0.72 m, whereas the corresponding value obtained from the proposed 17-DOF discrete model was approximately 0.69 m.

The dynamic responses predicted by both models exhibited very similar transient characteristics and converged to nearly identical steady-state deflection values. The maximum difference between the two models was approximately 0.035 m, corresponding to a relative error of 4.86%. This level of agreement demonstrates that the proposed reduced-order model is capable of accurately reproducing the global deformation behavior of the tower crane. Furthermore, the results confirm that the

17-DOF discrete model can provide reliable predictions while requiring significantly lower computational effort than the elastic MATLAB/SimMechanics model.

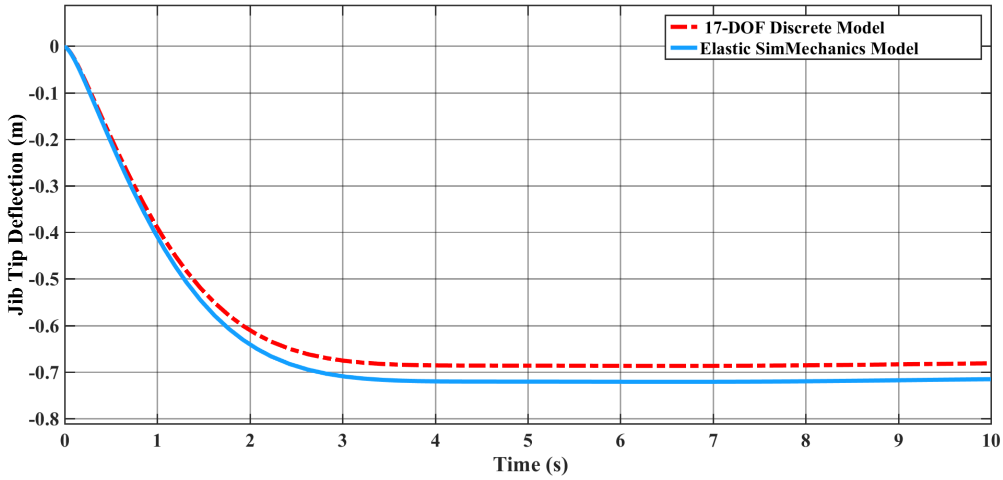

Figure 15. Comparison of the jib tip deflection responses predicted by the proposed 17-DOF discrete model and the elastic MATLAB/SimMechanics model under a 2-t concentrated tip load.

The close agreement between the reduced-order model and the elastic multibody model demonstrates that the proposed modeling approach can accurately capture the global structural response while significantly reducing the computational complexity.

4. Discussion

The structural and dynamic analyses performed in this study provide a comprehensive understanding of the behavior of a real flat-top tower crane under both static and free-vibration conditions. The finite element analyses demonstrated that all investigated structural components satisfied the allowable stress limits defined by the FEM 1.001 standard. Although the jib and counter-jib components exhibited the highest stress levels, the maximum equivalent stresses remained below the allowable limit of 240 MPa, indicating adequate structural safety under the most critical loading condition.

The findings obtained in the present study are generally consistent with previously reported tower crane investigations. Similar to the studies conducted by Huang et al. [11], Lei et al. [12], and Guo and Chen [13], the modal analyses revealed that the dynamic behavior of tower crane structures is strongly governed by the stiffness distribution of individual structural components. Furthermore, the static stress and displacement results obtained from the finite element analyses are in agreement with the observations reported by Gerdemeli et al. [5], Qing and Zeng [7], and Zhang et al. [10], who demonstrated that finite element methods provide reliable predictions of the structural performance of tower crane systems under operational loading conditions. The consistency between the present findings and those available in the literature further supports the validity of the adopted modeling approach.

The displacement results revealed that the largest deformation occurred at the jib tip. This behavior is expected because the jib acts as a long cantilever beam subjected to concentrated loading at its free end. Nevertheless, the obtained displacement was found to be compatible with the reverse camber introduced during the design stage.

This observation confirms the effectiveness of the design approach adopted by the manufacturer and demonstrates that the structural response of the crane remains within acceptable serviceability limits.

The modal analysis results further highlighted the importance of evaluating the dynamic characteristics of tower crane components individually. For all investigated subcomponents, the first six vibration modes corresponded to rigid-body motions, whereas the seventh mode represented the first elastic deformation mode. The obtained natural frequencies indicate that most structural components possess sufficient stiffness and are unlikely to experience resonance under normal operating conditions. However, the relatively low first elastic natural frequency identified for the counter-jib suggests that this component is more susceptible to dynamic excitation than the remaining structural members. Therefore, additional stiffness enhancement or structural optimization studies may be beneficial for improving its dynamic performance.

A significant contribution of the present study is the development of a 17-DOF discrete parameter model representing the global dynamic behavior of the tower crane. Unlike conventional finite element models, which generally require substantial computational effort, the proposed reduced-order formulation provides a computationally efficient alternative while preserving the dominant structural characteristics of the system. The stiffness parameters used in the mathematical model were derived directly from finite element analyses, enabling the reduced-order model to maintain a close physical relationship with the actual structure.

The validity of the proposed mathematical formulation was assessed through comparison with an elastic MATLAB/SimMechanics model developed using the actual mass and inertia properties of the crane. Under the application of a 2-t payload at the jib tip, the predicted steady-state tip deflections of both models showed excellent agreement. The maximum tip deflection obtained from the 17-DOF model was approximately 0.69 m, whereas the elastic SimMechanics model predicted a value of approximately 0.72 m. The resulting difference was approximately 4.2%, demonstrating that the reduced-order model is capable of accurately representing the global deformation behavior of the crane despite its significantly lower computational complexity.

Compared with previous studies available in the literature, which predominantly focus either on detailed finite element analyses or simplified low-order dynamic models, the present work provides an integrated framework combining finite element analysis, modal characterization, reduced-order mathematical modeling, and elastic multibody simulation. This integrated approach enables both structural assessment and dynamic evaluation within a unified methodology and provides a practical basis for future control, optimization, vibration suppression, and structural health monitoring studies of tower crane systems.

Overall, the results demonstrate that the proposed methodology can successfully represent the structural and dynamic behavior of real flat-top tower cranes. The developed reduced-order model offers a reliable and computationally efficient tool that can be utilized in future investigations involving active control applications, wind-induced vibration analyses, seismic response evaluation, and structural optimization studies. In addition to environmental loading, recent investigations have shown that the interaction among operating parameters significantly influences crane vibration characteristics and payload swing [31]. Drawing inspiration from vibration mitigation strategies proposed for smart civil engineering structures [32], the reduced-order model developed in this study may also provide a suitable platform for future active vibration control applications. Moreover, integrating finite element analysis with complementary computational frameworks such as computational fluid dynamics (CFD) and building information modeling (BIM) has been demonstrated to enhance structural optimization, computational efficiency, and design interoperability in large-scale structural systems [33]. Recent studies have demonstrated that integrated computational approaches combining finite element analysis with other numerical techniques can significantly improve structural optimization workflows [34]. Such multidisciplinary approaches may also be adopted for future tower crane design studies.

5. Conclusion

In this study, a comprehensive structural and dynamic analysis of a real 60/15 flat-top tower crane was carried out. Finite element analyses were performed to investigate the stress distribution, deformation behavior, and modal characteristics of the main structural components. Based on these analyses, a 17-degree-of-freedom (17-DOF) reduced-order mathematical model was developed using finite element-derived structural parameters and validated using an independent elastic multibody model created in MATLAB/SimMechanics. The comparison between the two models showed a maximum relative error of only 4.86% in the predicted jib tip deflection, confirming that the proposed reduced-order model can accurately represent the global structural response of the crane.

The modal analyses showed that the first six modes corresponded to rigid-body motions, whereas the seventh mode represented the first elastic deformation mode of each structural component. Among the investigated components, the counter-jib exhibited the lowest natural frequency, indicating that it is the most flexible part of the crane and may benefit from further structural optimization. The results also demonstrated that the proposed reduced-order model provides an efficient alternative to detailed finite element analyses while preserving the essential structural characteristics of the crane. Consequently, the developed modeling approach can be used as a practical basis for structural analysis, vibration assessment, controller development, and other engineering studies involving real flat-top tower crane systems.

The scope of this study was limited to the development and validation of a reduced-order model based on finite element-derived structural parameters. Experimental validation, full-system modal analysis, mesh convergence investigations, and advanced damping formulations such as Rayleigh damping were beyond the scope of the present work. Future studies should address these aspects to further improve the applicability of the proposed modeling approach. In addition, structural health monitoring techniques based on vision systems or unmanned aerial vehicle (UAV)-assisted inspections may be integrated to evaluate the dynamic condition of tower crane structures during service.

Author contributions: Conceptualization, MT; methodology, MT; software, MT and AÇ; validation, MT and AÇ; formal analysis, MT; investigation, MT and AÇ; resources, MT; data curation, AÇ; writing—original draft preparation, MT; writing—review and editing, MT; visualization, AÇ and MT; supervision, MT; project administration, MT. Both authors have read and agreed to the published version of the manuscript.

Funding: This research received no external funding.

Institutional review board statement: Not applicable.

Informed consent statement: Not applicable.

Data availability statement: The data used in this study are available from the corresponding author upon reasonable request.

Acknowledgment: The authors would like to thank Arnikon Engineering Inc. for providing access to the tower crane model and for their valuable technical support and contributions throughout the study.

Conflict of interest: The authors declare no conflict of interest. The present study is based on the M.Sc. thesis of the first author, entitled *Structural Analysis and Control of Tower Crane System* (Thesis No. 951087), completed at the Department of Mechanical Engineering, Graduate School of Natural and Applied Sciences, Necmettin Erbakan University, Türkiye, in 2025 [35]. The results presented in this paper constitute a part of the comprehensive structural and dynamic investigations carried out within that thesis.

AI use statement: During the preparation of this work, the authors used ChatGPT (OpenAI) for English-language editing to improve the clarity and readability of the manuscript. The authors subsequently reviewed and edited the content as necessary and take full responsibility for the final content of the published article.

References

1. Augustyn M, Barski M. Numerical and analytical determination of the critical wind speed causing the overturning of the top-slewing tower crane. Applied Sciences. 2025; 15(9): 4683. doi: 10.3390/app15094683
2. Chen W, Qin X, Yang Z, et al. Wind-induced tower crane vibration and safety evaluation. Journal of Low Frequency Noise, Vibration and Active Control. 2020; 39(2): 297–312. doi: 10.1177/1461348419847306
3. EN 1991-1-4. Eurocode 1: Actions on Structures–Part 1-4: General Actions–Wind Actions. 2010.
4. Federation Europeenne de la Manutention. FEM 1.001: Rules for the Design of Hoisting Appliances, 3rd ed. Federation Europeenne de la Manutention; 1998.
5. Gerdemeli I, Kurt S, Deliktaş O. Finite element analysis of the tower crane. In: Proceedings of the 14th International Research/Expert Conference on Trends in the Development of Machinery and Associated Technology; 11–18 September 2010; Mediterranean Cruise, Turkey. pp. 11–18.
6. Gu YQ, Wang WF, Guo SD. Analysis on tower crane under wind load by ANSYS. Applied Mechanics and Materials. 2012; 226–228: 35–38. doi: 10.4028/www.scientific.net/AMM.226-228.35
7. Qing L, Zeng YH. Finite element analysis on tower crane based on ANSYS. Applied Mechanics and Materials. 2012; 190–191: 373–380. doi: 10.4028/www.scientific.net/AMM.190-191.373
8. Karpe A, Karpe S, Chawrai A, et al. Validation of use of FEM (ANSYS) for structural analysis of tower crane jib and static and dynamic analysis of tower crane jib using ANSYS. International Journal of Innovative Research in Applied Engineering. 2014; 1(4): 69–75.
9. Zeng G, Chen K, Wang Y, et al. Stress and strain analysis and parameter optimization of pipe truss tower connection

of super-large tower crane based on FEM. Scientific Reports. 2024; 14(1): 3670. doi: 10.1038/s41598-024-54351-y
10. Zhang Q, Mei B, Yang H, et al. Stress measurement and analysis of structural parameters of flat arm tower crane under different working conditions. Buildings. 2025; 15(7): 1137. doi: 10.3390/buildings15071137
11. Huang GJ, He CZ, Wang XH. A modal analysis of giant shipbuilding tower crane. Applied Mechanics and Materials. 2013; 239–240: 473–477. doi: 10.4028/www.scientific.net/AMM.239-240.473
12. Lei JF, Chen XH, Huang L, et al. Modeling and modal analysis of the whole structure of PT7032 tower crane based on finite element method. Advanced Materials Research. 2013; 706–708: 1433–1436. doi: 10.4028/www.scientific.net/AMR.706-708.1433
13. Guo H, Chen K. Modal and fatigue characteristics analysis of key components of tower crane. Vibroengineering Procedia. 2024; 54: 72–77. doi: 10.21595/vp.2024.23826
14. Trong DX, Toan LK, Ngoc HT, et al. Modal analysis of cracked tower crane with an experimental validation. Vietnam Journal of Science and Technology. 2020; 58(6): 776–788. doi: 10.15625/2525-2518/58/6/15298
15. Jiang H, Li S. The wind-induced vibration response for tower crane based on virtual excitation method. Open Mechanical Engineering Journal. 2014; 8: 201–205.
16. Jiang H, Li Y. Dynamic reliability analysis of tower crane with wind loading. IOP Conference Series: Materials Science and Engineering. 2019; 677(5): 052031. doi: 10.1088/1757-899X/677/5/052031
17. Lu Y, Gao M, Liang T, et al. Wind-induced vibration assessment of tower cranes attached to high-rise buildings under construction. Automation in Construction. 2022; 135: 104132. doi: 10.1016/j.autcon.2022.104132
18. Oliveira CS, Correia PMB. Comparison of the seismic and wind analyses of two tower cranes. Journal of Vibroengineering. 2021; 23(4): 956–975. doi: 10.21595/jve.2021.21649
19. Liu F, Yang J, Wang J, et al. Effect on tower crane structural vibration under the lifting-luffing coupling condition. Journal of Mechanical Science and Technology. 2023; 37(10): 4935–4947. doi: 10.1007/s12206-023-0702-4
20. Rauscher F, Sawodny O. An elastic jib model for the slewing control of tower cranes. IFAC-PapersOnLine. 2017; 50(1): 9796–9801. doi: 10.1016/j.ifacol.2017.08.886
21. Stölzner M, Kleeberger M, Moll M, et al. Investigation of the dynamic loads on tower cranes during slewing operations. In: Proceedings of the 10th International Conference on Simulation and Modeling Methodologies, Technologies and Applications (SIMULTECH); 8–10 July 2020; Online. pp. 59–67. doi: 10.5220/0009816300590067
22. Yang Y, Zhang Z, Xu L, et al. Mechanical performance and failure mode research on the braced frame joint of tower cranes in high-rise building construction. Frontiers in Materials. 2022; 9: 824693. doi: 10.3389/fmats.2022.824693
23. Yang ZJ, Ai ZD, An HW. Mechanics analysis of tower crane. Applied Mechanics and Materials. 2014; 580–583: 3034–3037. doi: 10.4028/www.scientific.net/AMM.580-583.3034
24. Gu YQ, Mao CF. The preliminary analysis on tower crane by earthquake effect. Applied Mechanics and Materials. 2013; 353–356: 1892–1895. doi: 10.4028/www.scientific.net/AMM.353-356.1892
25. Kenan H, Azeloğlu O. Design of scaled down model of a tower crane mast by using similitude theory. Engineering Structures. 2020; 220: 110985. doi: 10.1016/j.engstruct.2020.110985
26. Zhu L, Wang Y. Static analysis and modal analysis of crane arms of tower cranes based on ANSYS. In: Proceedings of 9th International Conference on Mechanical Engineering, Materials, and Automation Technology (MMEAT 2023); 9–11 June 2023; Dalian, China. doi: 10.1117/12.3007715
27. Hric S, Tkac J, Matiskova D, et al. Preliminary analysis of tower crane as a type of truss structure. MATEC Web of Conferences. 2019; 299: 03003. doi: 10.1051/matecconf/201929903003
28. Hou C, Liu C, Li Z, et al. Tower crane systems modeling and adaptive robust sliding mode control design under unknown frictions and wind disturbances. Transactions of the Institute of Measurement and Control. 2025; 47(4): 795–809. doi: 10.1177/01423312241260911
29. Yu Z, Gu Z, Lan P, et al. Multibody system dynamic modeling and order reduction of tower crane. Journal of Dynamics and Control. 2024; 22(8): 58–65. doi: 10.6052/1672-6553-2024-023 (in Chinese)
30. Yu Z, Li H. A novel flexible multibody system dynamic analysis platform of tower crane. Machines. 2025; 13(12): 1103. doi: 10.3390/machines13121103
31. Liu P, Zhao C, Sun Y, et al. Impact of multiple operating parameter interactions on load swing of tower cranes. Machines. 2025; 13(2): 85. doi: 10.3390/machines13020085
32. Chitaoui H, Megnounif A, Benadla Z. Optimal Placement of Vibration Control Systems in a Smart Civil Engineering Structure. Civil Engineering Journal. 2025; 11(8): 3495–3515. doi: 10.28991/CEJ-2025-011-08-022
33. Abdelrheem AE, El-Helloty A, Ehab A. Integrated FEM, CFD, and BIM Approaches for Optimizing Pre-Stressed

Concrete Wind Turbine Tower Design. Civil Engineering Journal. 2025; 11(2): 523–543. doi: 10.28991/CEJ-2025-011-02-08
34. Chu TSC, Sorilla J, Chua AY. UAV-Based Structural Health Monitoring Using a Two-Stage CNN Model with Lighthouse Localization in GNSS-Denied Environments. HighTech and Innovation Journal. 2025; 6(2): 398–410. doi: 10.28991/HIJ-2025-06-02-03
35. Çoban A. Structural Analysis and Control of Tower Crane System [Master's thesis]. Necmettin Erbakan University; 2025.

Appendix A. Equations of motion of the proposed 17-degree-of-freedom discrete model

Base frame equation of motion:

$$m_s\ddot{x}_s + c_0\dot{x}_s + c_1\left(\dot{x}_s - \dot{x}_{sb}\right) + k_0x_s + k_1\left(x_s - x_{sb}\right) = 0$$

Super booster equation of motion:

$$m_{sb}\ddot{x}_{sb} + c_1\left(\dot{x}_{sb} - \dot{x}_s\right) + c_2\left(\dot{x}_{sb} - \dot{x}_b\right) + k_1\left(x_{sb} - x_s\right) + k_2\left(x_{sb} - x_b\right) = 0$$

Booster equation of motion:

$$m_b\ddot{x}_b + c_2\left(\dot{x}_b - \dot{x}_{sb}\right) + c_3\left(\dot{x}_b - \dot{x}_m\right) + k_2\left(x_b - x_{sb}\right) + k_3\left(x_b - x_m\right) = 0$$

Master equation of motion:

$$m_m\ddot{x}_m + c_3\left(\dot{x}_m - \dot{x}_b\right) + c_4\left(\dot{x}_m - \dot{x}_{km1}\right) + k_3\left(x_m - x_b\right) + k_4\left(x_m - x_{km1}\right) = 0$$

Short mast-1 equation of motion:

$$m_{km1}\ddot{x}_{km1} + c_4\left(\dot{x}_{km1} - \dot{x}_m\right) + c_5\left(\dot{x}_{km1} - \dot{x}_{km2}\right) + k_4\left(x_{km1} - x_m\right) + k_5\left(x_{km1} - x_{km2}\right) = 0$$

Short mast-2 equation of motion:

$$m_{km2}\ddot{x}_{km2} + c_5\left(\dot{x}_{km2} - \dot{x}_{km1}\right) + c_6\left(\dot{x}_{km2} - \dot{x}_k\right) + k_5\left(x_{km2} - x_{km1}\right) + k_6\left(x_{km2} - x_k\right) = 0$$

Tower–slewing platform equation of motion (for x):

$$m_k\ddot{x}_k + c_6\left(\dot{x}_k - \dot{x}_{km2}\right) + c_c\left(\dot{x}_k - \dot{y}_k\right) + k_6\left(x_k - x_{km2}\right) + k_c\left(x_k - y_k\right) = 0$$

Counter-jib equation of motion (for x):

$$m_{ky}\ddot{y}_{ky} + c_7\left(\dot{y}_{ky} - \dot{y}_k\right) + k_7\left(y_{ky} - y_k\right) = 0$$

Tower–slewing platform equation of motion (for y):

$$m_k\ddot{y}_k + c_7\left(\dot{y}_k - \dot{y}_{ky}\right) + c_8\left(\dot{y}_k - \dot{y}_k\right) + c_c\left(\dot{y}_k - \dot{x}_k\right) + k_7\left(y_k - y_{ky}\right) + k_8\left(y_k - y_{b1}\right) + k_c\left(y_k - x_k\right) = 0$$

Jib-1 equation of motion:

$$m_{b1}\ddot{y}_{b1} + c_8\left(\dot{y}_{b1} - \dot{y}_k\right) + c_9\left(\dot{y}_{b1} - \dot{y}_{b2}\right) + k_8\left(y_{b1} - y_k\right) + k_9\left(y_{b1} - y_{b2}\right) = 0$$

Jib-2 equation of motion:

$$m_{b2}\ddot{y}_{b2} + c_9(\dot{y}_{b2} - \dot{y}_{b1}) + c_{10}(\dot{y}_{b2} - \dot{y}_{b3}) + k_9(y_{b2} - y_{b1}) + k_{10}(y_{b2} - y_{b3}) = 0$$

Jib-3 equation of motion:

$$m_{b3}\ddot{y}_{b3} + c_{10}(\dot{y}_{b3} - \dot{y}_{b2}) + c_{11}(\dot{y}_{b3} - \dot{y}_{b4}) + k_{10}(y_{b3} - y_{b2}) + k_{11}(y_{b3} - y_{b4}) = 0$$

Jib-4 equation of motion:

$$m_{b4}\ddot{y}_{b4} + c_{11}(\dot{y}_{b4} - \dot{y}_{b3}) + c_{12}(\dot{y}_{b4} - \dot{y}_{b5}) + k_{11}(y_{b4} - y_{b3}) + k_{12}(y_{b4} - y_{b5}) = 0$$

Jib-5 equation of motion:

$$m_{b5}\ddot{y}_{b5} + c_{12}(\dot{y}_{b5} - \dot{y}_{b4}) + c_{13}(\dot{y}_{b5} - \dot{y}_{b6}) + k_{12}(y_{b5} - y_{b4}) + k_{13}(y_{b5} - y_{b6}) = 0$$

Jib-6 equation of motion:

$$m_{b6}\ddot{y}_{b6} + c_{13}(\dot{y}_{b6} - \dot{y}_{b5}) + c_{14}(\dot{y}_{b6} - \dot{y}_{b7}) + k_{13}(y_{b6} - y_{b5}) + k_{14}(y_{b6} - y_{b7}) = 0$$

Jib-7 equation of motion:

$$m_{b7}\ddot{y}_{b7} + c_{14}(\dot{y}_{b7} - \dot{y}_{b6}) + c_{15}(\dot{y}_{b7} - \dot{y}_{b8}) + k_{14}(y_{b7} - y_{b6}) + k_{15}(y_{b7} - y_{b8}) = 0$$

Jib-8 equation of motion:

$$m_{b8}\ddot{y}_{b8} + c_{15}(\dot{y}_{b8} - \dot{y}_{b7}) + k_{15}(y_{b8} - y_{b7}) = F(t)$$

Appendix B. *M, C,* and *K* matrices

$$M = \begin{bmatrix}
m_s & 0 & 0 & 0 & 0 & 0 & 0 & 0 & 0 & 0 & 0 & 0 & 0 & 0 & 0 & 0 & 0 \\
0 & m_{sb} & 0 & 0 & 0 & 0 & 0 & 0 & 0 & 0 & 0 & 0 & 0 & 0 & 0 & 0 & 0 \\
0 & 0 & m_b & 0 & 0 & 0 & 0 & 0 & 0 & 0 & 0 & 0 & 0 & 0 & 0 & 0 & 0 \\
0 & 0 & 0 & m_m & 0 & 0 & 0 & 0 & 0 & 0 & 0 & 0 & 0 & 0 & 0 & 0 & 0 \\
0 & 0 & 0 & 0 & m_{km1} & 0 & 0 & 0 & 0 & 0 & 0 & 0 & 0 & 0 & 0 & 0 & 0 \\
0 & 0 & 0 & 0 & 0 & m_{km2} & 0 & 0 & 0 & 0 & 0 & 0 & 0 & 0 & 0 & 0 & 0 \\
0 & 0 & 0 & 0 & 0 & 0 & m_k & 0 & 0 & 0 & 0 & 0 & 0 & 0 & 0 & 0 & 0 \\
0 & 0 & 0 & 0 & 0 & 0 & 0 & m_{ky} & 0 & 0 & 0 & 0 & 0 & 0 & 0 & 0 & 0 \\
0 & 0 & 0 & 0 & 0 & 0 & 0 & 0 & m_k & 0 & 0 & 0 & 0 & 0 & 0 & 0 & 0 \\
0 & 0 & 0 & 0 & 0 & 0 & 0 & 0 & 0 & m_{b1} & 0 & 0 & 0 & 0 & 0 & 0 & 0 \\
0 & 0 & 0 & 0 & 0 & 0 & 0 & 0 & 0 & 0 & m_{b2} & 0 & 0 & 0 & 0 & 0 & 0 \\
0 & 0 & 0 & 0 & 0 & 0 & 0 & 0 & 0 & 0 & 0 & m_{b3} & 0 & 0 & 0 & 0 & 0 \\
0 & 0 & 0 & 0 & 0 & 0 & 0 & 0 & 0 & 0 & 0 & 0 & m_{b4} & 0 & 0 & 0 & 0 \\
0 & 0 & 0 & 0 & 0 & 0 & 0 & 0 & 0 & 0 & 0 & 0 & 0 & m_{b5} & 0 & 0 & 0 \\
0 & 0 & 0 & 0 & 0 & 0 & 0 & 0 & 0 & 0 & 0 & 0 & 0 & 0 & m_{b6} & 0 & 0 \\
0 & 0 & 0 & 0 & 0 & 0 & 0 & 0 & 0 & 0 & 0 & 0 & 0 & 0 & 0 & m_{b7} & 0 \\
0 & 0 & 0 & 0 & 0 & 0 & 0 & 0 & 0 & 0 & 0 & 0 & 0 & 0 & 0 & 0 & m_{b8}
\end{bmatrix}$$

$$C=\left[\begin{array}{ccccccccccccccccc}
c0+c1 & -c1 & 0 & 0 & 0 & 0 & 0 & 0 & 0 & 0 & 0 & 0 & 0 & 0 & 0 & 0 & 0\\
-c1 & c1+c2 & -c2 & 0 & 0 & 0 & 0 & 0 & 0 & 0 & 0 & 0 & 0 & 0 & 0 & 0 & 0\\
0 & -c2 & c2+c3 & -c3 & 0 & 0 & 0 & 0 & 0 & 0 & 0 & 0 & 0 & 0 & 0 & 0 & 0\\
0 & 0 & -c3 & c3+c4 & -c4 & 0 & 0 & 0 & 0 & 0 & 0 & 0 & 0 & 0 & 0 & 0 & 0\\
0 & 0 & 0 & -c4 & c4+c5 & -c5 & 0 & 0 & 0 & 0 & 0 & 0 & 0 & 0 & 0 & 0 & 0\\
0 & 0 & 0 & 0 & -c5 & c5+c6 & -c6 & 0 & 0 & 0 & 0 & 0 & 0 & 0 & 0 & 0 & 0\\
0 & 0 & 0 & 0 & 0 & -c6 & c6+cc & 0 & -cc & 0 & 0 & 0 & 0 & 0 & 0 & 0 & 0\\
0 & 0 & 0 & 0 & 0 & 0 & 0 & c7 & -c7 & 0 & 0 & 0 & 0 & 0 & 0 & 0 & 0\\
0 & 0 & 0 & 0 & 0 & 0 & -cc & -c7 & c7+c8+cc & -c8 & 0 & 0 & 0 & 0 & 0 & 0 & 0\\
0 & 0 & 0 & 0 & 0 & 0 & 0 & 0 & -c8 & c8+c9 & -c9 & 0 & 0 & 0 & 0 & 0 & 0\\
0 & 0 & 0 & 0 & 0 & 0 & 0 & 0 & 0 & -c9 & c9+c10 & -c10 & 0 & 0 & 0 & 0 & 0\\
0 & 0 & 0 & 0 & 0 & 0 & 0 & 0 & 0 & 0 & -c10 & c10+c11 & -c11 & 0 & 0 & 0 & 0\\
0 & 0 & 0 & 0 & 0 & 0 & 0 & 0 & 0 & 0 & 0 & -c11 & c11+c12 & -c12 & 0 & 0 & 0\\
0 & 0 & 0 & 0 & 0 & 0 & 0 & 0 & 0 & 0 & 0 & 0 & -c12 & c12+c13 & -c13 & 0 & 0\\
0 & 0 & 0 & 0 & 0 & 0 & 0 & 0 & 0 & 0 & 0 & 0 & 0 & -c13 & c13+c14 & -c14 & 0\\
0 & 0 & 0 & 0 & 0 & 0 & 0 & 0 & 0 & 0 & 0 & 0 & 0 & 0 & -c14 & c14+c15 & -c15\\
0 & 0 & 0 & 0 & 0 & 0 & 0 & 0 & 0 & 0 & 0 & 0 & 0 & 0 & 0 & -c15 & c15
\end{array}\right]$$

$$K=\left[\begin{array}{ccccccccccccccccc}
k0+k1 & -k1 & 0 & 0 & 0 & 0 & 0 & 0 & 0 & 0 & 0 & 0 & 0 & 0 & 0 & 0 & 0\\
-k1 & k1+k2 & -k2 & 0 & 0 & 0 & 0 & 0 & 0 & 0 & 0 & 0 & 0 & 0 & 0 & 0 & 0\\
0 & -k2 & k2+k3 & -k3 & 0 & 0 & 0 & 0 & 0 & 0 & 0 & 0 & 0 & 0 & 0 & 0 & 0\\
0 & 0 & -k3 & k3+k4 & -k4 & 0 & 0 & 0 & 0 & 0 & 0 & 0 & 0 & 0 & 0 & 0 & 0\\
0 & 0 & 0 & -k4 & k4+k5 & -k5 & 0 & 0 & 0 & 0 & 0 & 0 & 0 & 0 & 0 & 0 & 0\\
0 & 0 & 0 & 0 & -k5 & k5+k6 & -k6 & 0 & 0 & 0 & 0 & 0 & 0 & 0 & 0 & 0 & 0\\
0 & 0 & 0 & 0 & 0 & -k6 & k6+kc & 0 & -kc & 0 & 0 & 0 & 0 & 0 & 0 & 0 & 0\\
0 & 0 & 0 & 0 & 0 & 0 & 0 & k7 & -k7 & 0 & 0 & 0 & 0 & 0 & 0 & 0 & 0\\
0 & 0 & 0 & 0 & 0 & 0 & -kc & -k7 & k7+k8+kc & -k8 & 0 & 0 & 0 & 0 & 0 & 0 & 0\\
0 & 0 & 0 & 0 & 0 & 0 & 0 & 0 & -k8 & k8+k9 & -k9 & 0 & 0 & 0 & 0 & 0 & 0\\
0 & 0 & 0 & 0 & 0 & 0 & 0 & 0 & 0 & -k9 & k9+k10 & -k10 & 0 & 0 & 0 & 0 & 0\\
0 & 0 & 0 & 0 & 0 & 0 & 0 & 0 & 0 & 0 & -k10 & k10+k11 & -k11 & 0 & 0 & 0 & 0\\
0 & 0 & 0 & 0 & 0 & 0 & 0 & 0 & 0 & 0 & 0 & -k11 & k11+k12 & -k12 & 0 & 0 & 0\\
0 & 0 & 0 & 0 & 0 & 0 & 0 & 0 & 0 & 0 & 0 & 0 & -k12 & k12+k13 & -k13 & 0 & 0\\
0 & 0 & 0 & 0 & 0 & 0 & 0 & 0 & 0 & 0 & 0 & 0 & 0 & -k13 & k13+k14 & -k14 & 0\\
0 & 0 & 0 & 0 & 0 & 0 & 0 & 0 & 0 & 0 & 0 & 0 & 0 & 0 & -k14 & k14+k15 & -k15\\
0 & 0 & 0 & 0 & 0 & 0 & 0 & 0 & 0 & 0 & 0 & 0 & 0 & 0 & 0 & -k15 & k15
\end{array}\right]$$

Appendix C

Table A1. The numerical values of the calculated mass, stiffness, and damping coefficients.

Component	*M* (kg)	*C* (N.s/m)	*K* (N/m)
Base Frame	$(m_s) = 101{,}373$	$C_0 = 70{,}748$	$K_0 = 19{,}749{,}965$
Super Booster	$(m_{sb}) = 6{,}418$	$C_1 = 10{,}349$	$K_1 = 6{,}675{,}122$
Booster	$(m_b) = 497$	$C_2 = 9{,}110$	$K_2 = 6{,}675{,}122$
Master	$(m_m) = 4{,}400$	$C_3 = 8{,}569$	$K_3 = 6{,}675{,}122$
Short Mast-1	$(m_{km\text{-}1}) = 1{,}551$	$C_4 = 14{,}466$	$K_4 = 53{,}981{,}107$
Short Mast-2	$(m_{km\text{-}2}) = 1{,}555$	$C_5 = 14{,}487$	$K_5 = 53{,}981{,}107$
Tower–Slewing	$(m_k) = 7{,}634$	$C_6 = 40{,}696$	$K_6 = 86{,}775{,}425$
Tower–Slewing	$(m_k) = 7{,}634$	$C_c = 1{,}797$	$K_c = 1 \times 10^6$
Counter-Jib	$(m_{ky}) = 27{,}386$	$C_7 = 3{,}721$	$K_7 = 202{,}224$
Jib-1	$(m_{b1}) = 3{,}438$	$C_8 = 2{,}010$	$K_8 = 470{,}256$
Jib-2	$(m_{b2}) = 2{,}493$	$C_9 = 1{,}536$	$K_9 = 378{,}659$
Jib-3	$(m_{b3}) = 1{,}888$	$C_{10} = 1{,}404$	$K_{10} = 417{,}659$
Jib-4	$(m_{b4}) = 712$	$C_{11} = 1{,}462$	$K_{11} = 1{,}199{,}861$
Jib-5	$(m_{b5}) = 656$	$C_{12} = 1{,}397$	$K_{12} = 1{,}190{,}420$
Jib-6	$(m_{b6}) = 558$	$C_{13} = 1{,}288$	$K_{13} = 1{,}189{,}400$
Jib-7	$(m_{b7}) = 325$	$C_{14} = 1{,}140$	$K_{14} = 1{,}599{,}156$
Jib-8	$(m_{b8}) = 398$	$C_{15} = 1{,}247$	$K_{15} = 1{,}563{,}893$